Journal of
Composites Science

MDPI

Article

Determining the Elastic Constants and Thickness of the Interphase in Fiberglass Plastic Composites from Micromechanical and Macromechanical Tests

Alexander Smirnov *, Evgeniya Smirnova, Dmitry Vichuzhanin, Yulia Khudorozhkova, Irina Spirina, Vladislav Kanakin and Olga Muizemnek

Institute of Engineering Science, Ural Branch of the Russian Academy of Sciences (UB RAS), 620049 Ekaterinburg, Russia
* Correspondence: smirnov@imach.uran.ru

Abstract: The aim of this paper is to describe a methodology for determining the elastic constants and thickness of the interphase between matrix and fiber in fiberglass plastic composites from macro- and micromechanical testing. Macromechanical testing is tension of unidirectional fiberglass plastics along and across the fiber direction. Micromechanical testing is tension of glass fibers and instrumented microindentation into the matrix and the fiberglass. The interphase thickness is determined by dynamic force microscopy on thin sections without a height difference. The measured interphase thickness is 621 nm. Based on the interphase thickness, a mesomechanical finite element model of a fiberglass monolayer is constructed. As a result, it is found that the elastic modulus and Poisson's ratio are 12.7 GPa, 0.07. It is established that the elastic properties of the interphase differ significantly from those of the matrix. The paper also explores the possibility of determining the interphase thickness through computational experiments. It turns out that by knowing the actual elastic properties of the matrix and the fiber, as well as the fiberglass monolayer, it is feasible to calculate the interphase and its elastic properties with acceptable engineering accuracy. The deviation of the calculated interphase thickness from the experimentally measured one is 6%.

Keywords: polymer composite; interphase; mesomechanical model; microindentation; dynamic force microscopy; mechanical properties

Academic Editor: Francesco Tornabene

Received: 15 November 2024
Revised: 14 January 2025
Accepted: 17 January 2025
Published: 23 January 2025

Citation: Smirnov, A.; Smirnova, E.; Vichuzhanin, D.; Khudorozhkova, Y.; Spirina, I.; Kanakin, V.; Muizemnek, O. Determining the Elastic Constants and Thickness of the Interphase in Fiberglass Plastic Composites from Micromechanical and Macromechanical Tests. *J. Compos. Sci.* **2025**, *9*, 54. https://doi.org/10.3390/jcs9020054

1. Introduction

Reducing the weight of structures by using materials with high specific strength is a current research trend aimed at improving the energy efficiency of vehicles. Therefore, polymer composites reinforced with high-strength fibers have become widespread in the aerospace industry. As a rule, fibers made of glass, carbon, ceramics, aramid, and natural materials are used as reinforcing fibers [1–3]. The most widespread composites are polymer composites reinforced with glass and carbon fibers. The composite matrix is a very important part of polymer matrix composites since it transfers loads to fibers and distributes stresses among them. It also protects the fibers from environmental influences and has an effect on fiber location [4–6]. An interphase appears between the matrix and the fibers during matrix polymerization [7–11]. This zone generally differs significantly in composition from the matrix phase since it incorporates the finishing agent, the lubricant, and other low-molecular-weight inclusions of the binder and the filler surface. The structural differences resulting from the influence of the filler appear as a change in the degree of cure

in some cases and as a change in the degree of grain formation in the adjacent polymer in others. The interphase transfers stresses from the matrix to the fiber and, therefore, it makes an important contribution to the transfer of stresses among the fibers themselves, and it has a significant effect on the mechanical properties of composites. A strong bond between the fiber and the matrix causes high stiffness and strength, while a relatively weak interphase bond usually improves the energy-absorption characteristics under impact conditions. Thus, the ability to determine the properties of the interphase allows us to investigate the effect of polymerization conditions, the matrix composition, and the finishing agent on the mechanical properties of the interphase. This means that it becomes possible to design a composite product with tailored mechanical properties of the interphase and, as a result, to control the mechanical properties of the composite product. In addition to affecting the mechanical properties (elastic modulus, Poisson's ratio), the interphase has a significant effect on the ultimate strength of a polymer matrix composite material and on the initiation and evolution of cracks in it [12–16]. This necessitates taking into account explicitly the interphase in calculations aimed at determining conditions for the formation and evolution of cracks at the meso level. Finite element models are often used for this purpose. They describe the elastic or elastic–plastic behavior of structurally inhomogeneous materials at the micro or meso level, in which the elastic constants and shapes of the phases are explicitly set [9,17,18].

Phase shapes can be determined by FIB–SEM tomography [19–22], dynamic mechanical mapping [10,23,24], and computed tomography [22,25–27], whereas it is a nontrivial problem to determine the elastic properties of the phases (Poisson's ratio and the normal elastic modulus) at the meso level. The most common method for determining mechanical properties at the meso level is the method of instrumented indentation and scratching, which allows us to determine the hardness of phases and the reduced elastic modulus and to reconstruct hardening curves [28–32]. The main disadvantage of the indentation method as applied to determining the elastic modulus is the necessity to know the Poisson's ratio of the material, which is often unknown for the phase under study. In terms of the elastic modulus of the interphase between the fiber and the polymer matrix in the composite, another disadvantage of the instrumented indentation method appears. It is associated with the requirement imposed on the phase environment. The imprint size after indentation into a phase should be significantly smaller than the phase size in all directions. In this case, there is almost no influence of the environment on the determined reduced elastic modulus of the phase.

Another problem in determining the shape and mechanical properties of the interphase in composites with matrices based on epoxy resins is the inability to observe it in the optically visible range of the wave spectrum, and this prevents indentation into the interphase. The above problems lead to the fact that the mechanical properties of the interphase in a polymer composite are calculated rather than experimentally determined. The calculations are made analytically [33,34] or by means of finite element [9,34–36] and molecular dynamic models [8,37,38]. With this approach, the calculated values of the mechanical properties of the interphase largely depend on the accuracy and correctness of determining the mechanical properties of the matrix and the reinforcing fibers. Since the fiber diameter in state-of-the-art polymer composites is within 10 μm, it is necessary to use micromechanical tests for the accurate determination of the mechanical properties of the fiber. The purpose of this study is, proceeding from micromechanical and macromechanical testing, to develop a methodical approach to determining the elastic constants and thickness of the interphase in fiberglass plastics.

2. Materials and Methods

A prepreg with unidirectional glass fibers and the ASM 102 epoxy binder was used as a starting material for the manufacture of fiberglass plastic. The curing of the binder included prepreg package heating to 125 °C between flat plates under a pressure of 0.6 MPa. The heating rate was 2 °C/min, and it was followed by holding at this temperature for 3 h. Then, the prepreg was cooled to room temperature at a rate of at most 3 °C/min. After curing, the volume content of the glass fibers in a monolayer, the size of the glass fibers, and glass fiber laying were determined. These measurements were based on optical microscopy data. Figure 1 shows fiber laying in the monolayer, the variation of fiber diameters, and stacking of layers in 14-layer cross-reinforced fiberglass plastic.

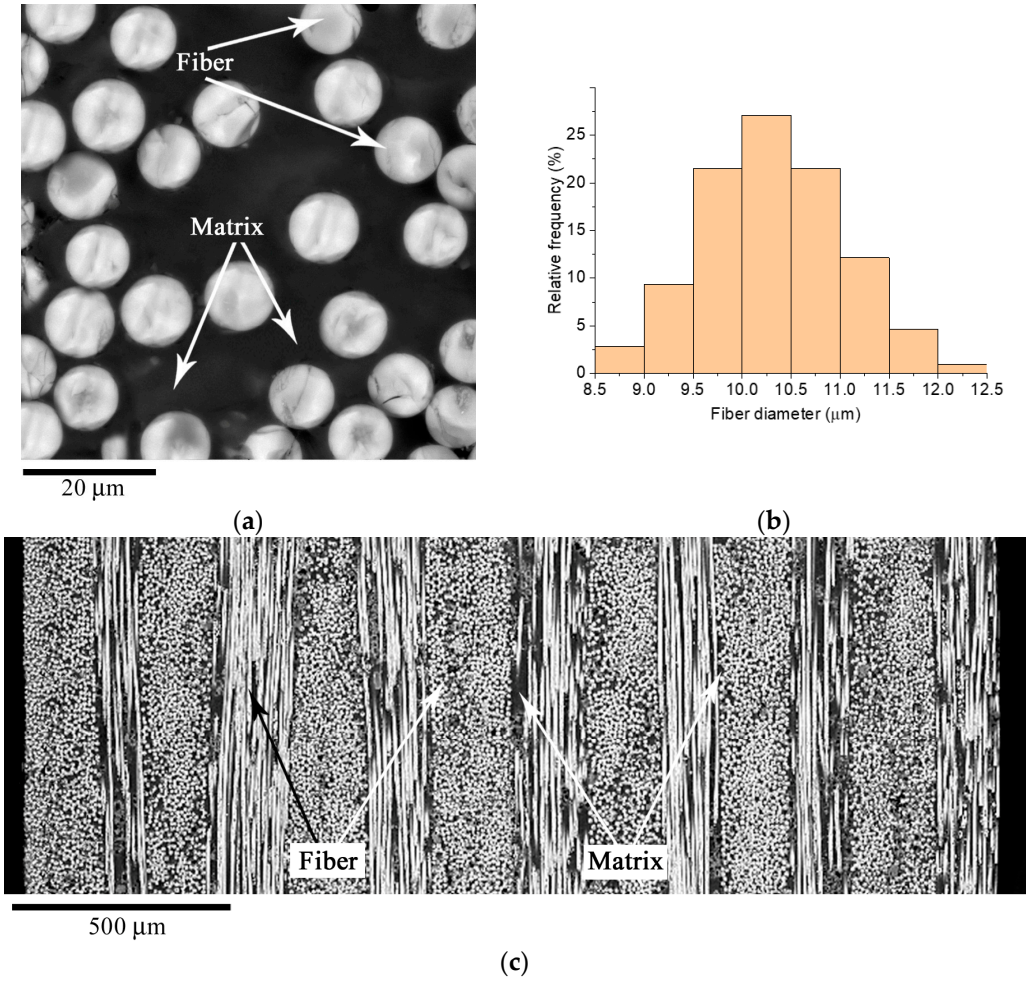

Figure 1. Fiber laying in a monolayer (**a**), fiber diameter variation (**b**), and laying of layers in a 14-layer fiberglass plastic (**c**).

According to the prepreg technology, two types of 14-layer fiberglass plastic panels were produced: with unidirectional laying and cross-reinforced. Tensile specimens were cut out from these panels, namely five specimens from cross-reinforced fiberglass plastic, five unidirectional specimens cut along the direction of laying, and five unidirectional specimens cut across the direction of laying. All the specimens had a length of 230 mm and a width of 25 mm. The tensile tests on a macro level were performed in an Instron 8801 (Illinois Tool Works Inc., Hopkinton, MA, USA) servo-hydraulic experimental testing machine. Deformations were measured directly on the specimen in two directions by means of an Instron AVE noncontact video extensometer, which ensured the absence of additional external influences on the specimen surface.

Indentation experiments were performed in a Hysitron TI950 (Bruker Corporation, Billerica, MA, USA) nanomechanical testing system using a Berkovich indenter. The Oliver–Pharr method underlying the ISO 14577 standard [39] for measuring hardness was used to determine the normal elastic modulus of the composite constituents. Indentation was performed on plane-parallel planes obtained by ion etching, which allows the properties of the structural constituents of the composite to be determined without introducing fragments and deformations into the surface during mechanical preparation. Ion etching was performed by means of SemPrep2 (Technoorg Linda, Budapest, Hungary) for 30 min at an accelerating voltage of 10 kV with the angle of specimen inclination to the ion beam equal to 7°. Before the start of ion etching, the polymer was cooled in an ion etching chamber to +1 °C.

Experiments on micromechanical tension of the single fiber were performed in the device shown in Figure 2. The elastic elongation of the loaded fiber was measured by means of a measuring microscope with a linear displacement measurement accuracy of 1 μm over a length of 1 mm. The base for measuring fiber elongation was about 10 mm. The microscope was used to measure the distance between the reference points on the fiber (base) at various axial load values. Graphite particles were the reference points (see Figure 2). They were placed on the fiber with a brush. The use of liquid colorants for painting the reference points on the fiber was not suitable due to the presence of surface tension in the colorant, which caused an underestimation of the elastic modulus and decreased the ultimate strength of the fiber. In order to determine the diameter of each fiber under test, the free end of the fiber was cut off, which was not in the grips of the tensile device. Then, each fiber was filled with epoxy resin separately from the others. Prior to this process, the fiber was arranged such that it passed through the resin in a direction perpendicular to the future cross-sectional plane. Subsequently, the thin section was made in the transverse direction of the fiber. The diameter of the fiber was then measured using an optical microscope.

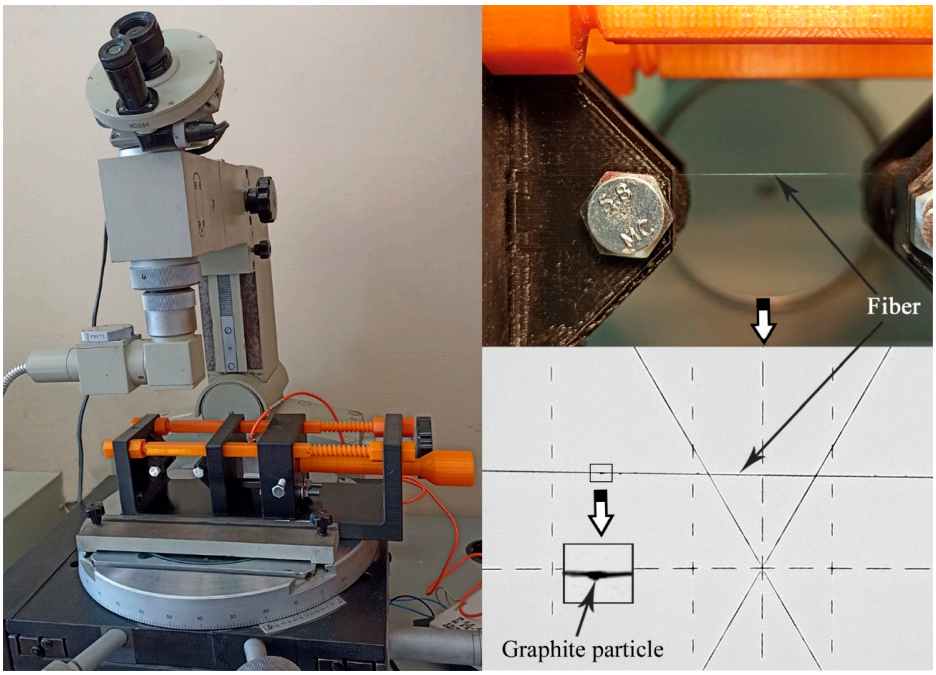

Figure 2. A device for tension of single micron-diameter fiber.

The size of the interphase was determined based on data obtained using an NT-206 (Microtestmachines, Gomel, Belarus) atomic force microscope in dynamic force microscopy mode. To prevent the influence of the surface relief on the oscillation amplitude and

resonant frequencies of an atomic force microscope cantilever, we performed analysis on a cross section made at an angle of 30° by burning the material with an ion beam. The burning was carried out on a SemPrep2 (Technoorg Linda, Budapest, Hungary) ion etching system. The process scheme of cutting the sample is shown in Figure 3a. As can be seen from Figure 3b, the fibers have an elliptical shape. In order to avoid the influence of the shape (stretching) of the fiber on the measured size of the interphase, we measured only along the line of the minor axis of the ellipse.

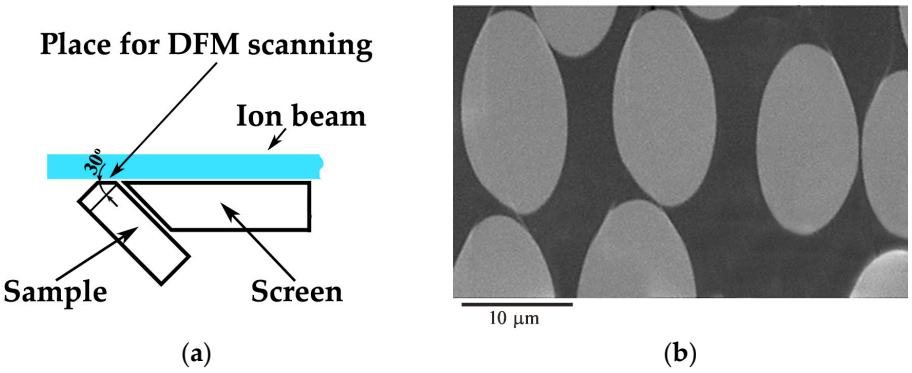

Figure 3. The scheme of obtaining a cross-section (**a**) and the shape of the fibers in the cross-section as seen through scanning electron microscopy (**b**).

3. The Procedure of Determining the Elastic Constants and Thickness of the Interphase in the Fiberglass Plastic

In this paper, the composite material under study is considered in terms of hierarchically organized systems [40–43], which are characterized by an interconnected reaction between adjacent scale levels as a result of external thermal deformation effects. The mesoscale level includes separate geometrically irregular structures, such as a matrix, an interphase, and reinforcing fibers with different laying directions, sizes, and spatial distributions. Based on the structure of the material under study, the macroscale level is considered as a multilayer material with uniform (averaged) properties in each monolayer, determined at the mesoscale level.

In this study, two problems were set. The first task was to calculate the elastic coefficients of the interphase. In order to do this, we needed to know its average thickness. This thickness was determined using atomic force microscopy. The second problem was to calculate the elastic coefficients and the interphase thickness. The purpose of this problem was to determine whether the interphase thickness can be reliably calculated based on the elastic properties of the fiber, matrix, and monolayers of the composite at the macro level.

In this study, the elastic constants of the interphase are determined indirectly, by calculating them from the solution of boundary value problems for tensing unidirectional fiberglass layers with regard to the experimentally determined properties of the matrix and fibers. Since the fibers are misoriented relative to the laying axis, the analytical model for determining the interphase should take into account fiber misorientation. This is a rather nontrivial problem. Therefore, in this study, the interphase parameters are determined by minimizing the deviation of the experimentally determined elastic constants of unidirectional fiberglass from the parameters calculated by the computational model describing the monolayer behavior at the meso level. In this case, the initial approximation of the properties and dimensions of the interphase for the computational model are the values obtained by the analytical model.

This section may be divided by subheadings. It should provide a concise and precise description of the experimental results, their interpretation, as well as the experimental conclusions that can be drawn.

3.1. The Analytical Model for Determining the Initial Elastic Interphase Parameters

In the statement of the composite deformation problem at the macroscale, it is assumed that the properties of the monolayer are described by the linear elastic orthotropic model [44–47]. The linear elastic isotropic model describes the mechanical properties of the structural constituents of the composite—the glass fiber, the polymer matrix, and the interphase. The generalized Hooke's law can be written for an orthotropic body as follows:

$$\begin{bmatrix} \varepsilon_x \\ \varepsilon_y \\ \varepsilon_z \\ 2\varepsilon_{yz} \\ 2\varepsilon_{zx} \\ 2\varepsilon_{xy} \end{bmatrix} = \begin{bmatrix} \frac{1}{E_x} & -\frac{\mu_{yx}}{E_y} & -\frac{\mu_{zx}}{E_z} & 0 & 0 & 0 \\ -\frac{\mu_{xy}}{E_x} & \frac{1}{E_y} & -\frac{\mu_{zy}}{E_z} & 0 & 0 & 0 \\ -\frac{\mu_{xz}}{E_x} & -\frac{\mu_{yz}}{E_y} & \frac{1}{E_z} & 0 & 0 & 0 \\ 0 & 0 & 0 & \frac{1}{G_{yz}} & 0 & 0 \\ 0 & 0 & 0 & 0 & \frac{1}{G_{xz}} & 0 \\ 0 & 0 & 0 & 0 & 0 & \frac{1}{G_{xy}} \end{bmatrix} \begin{bmatrix} \sigma_x \\ \sigma_y \\ \sigma_z \\ \sigma_{yz} \\ \sigma_{zx} \\ \sigma_{xy} \end{bmatrix}, \quad (1)$$

where ε_x, ε_y, ε_z, ε_{yz}, ε_{zx}, and ε_{xy} are the components of the strain vector $[\varepsilon]$; σ_x,σ_y, σ_z, σ_{yz}, σ_{zx}, and σ_{xy} are the components of the stress vector $[\sigma]$; E_x, E_y, and E_z are elastic moduli in the x, y, and z directions (the orientation of the axes is shown in Figure 4); G_{xy}, G_{yz}, and G_{xz} are the shear moduli in the xy, yz, and xz planes, respectively; and μ_{xy}, μ_{xz}, μ_{yx}, μ_{yz}, μ_{zx}, and μ_{zy} are Poisson's ratios.

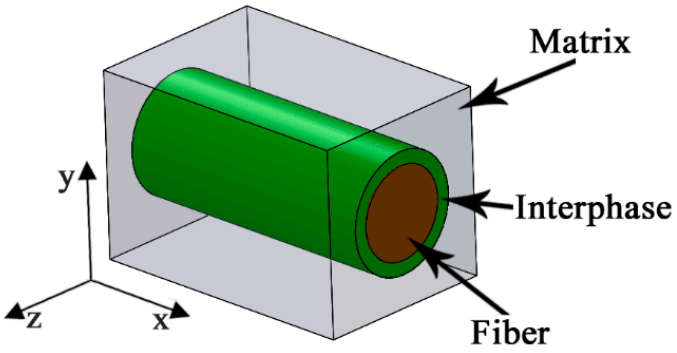

Figure 4. Orientation of the coordinate system relative to the laying axis.

Figure 4 shows coordinate system orientation relative to the laying axis. When constructing equations for determining the elastic modulus and the volume fraction of the interphase from tensile experiments, we assume that the phase structure is uniformly distributed along the x-axis. In this case, using the mixture rule [48–50] for uniaxial tension of the monolayer along the x-axis (along the fiber laying direction), we can write the following equation:

$$E_x = E^f \cdot \nu^f + E^m \cdot \nu^m + E^{in} \cdot \nu^{in}, \quad (2)$$

and for uniaxial tension along the y-axis (across the fiber laying direction), the following equation can be written:

$$\varepsilon_y = \varepsilon_y^f \cdot \nu^f + \varepsilon_y^m \cdot \nu^m + \varepsilon_y^{in} \cdot \nu^{in}, \quad (3)$$

where E_x and ε_y are the elastic modulus and the strain of the monolayer in Hooke's law (1), respectively; E^f, E^m, and E^{in} are the elastic moduli of the fiber, the matrix, and the

interphase, respectively; ν^f, ν^m, and ν^{in} are the volume fraction of the fiber, the matrix, and the interphase, respectively; and ε_y^f, ε_y^m, and ε_y^{in} are the strain of the fiber, the matrix, and the interphase along the y-direction during uniaxial tension of the monolayer along the y-axis. The volume fraction ν^f, ν^m, and ν^{in} must correspond to the following equality:

$$\nu^f + \nu^m + \nu^{in} = 1. \tag{4}$$

For uniaxial tension of the monolayer along the y-axis, the relationship of ε_y, σ_y, and E_y is $\varepsilon_y = \frac{\sigma_y}{E_y}$. Similar equalities can be written for the matrix, the interphase, and the fiber.

Also, in the case of uniaxial tension of the monolayer along the y-axis, the following equalities are true: $\sigma_y = \sigma_y^f = \sigma_y^m = \sigma_y^{in}$, where σ_y is the monolayer stress along the y-axis in Hooke's law (1); and σ_y^f, σ_y^m, and σ_y^{in} are the stresses of the fiber, the matrix, and the interphase along the y-axis in Hooke's law, respectively. Using the above equalities, Equation (3) can be written as

$$\frac{\sigma_y}{E_y} = \frac{\sigma^y}{E^f} \cdot \nu^f + \frac{\sigma^y}{E^m} \cdot \nu^m + \frac{\sigma^y}{E^{in}} \cdot \nu^{in}. \tag{5}$$

The fiber volume fraction and all the elastic constants of the monolayer, the glass fiber, and the matrix can be determined from tests at the macroscopic and microscopic scales. As a result, in the equation system consisting of Equations (2), (4), and (5), it is only the elastic modulus of the interphase E^{in} and its volume fraction ν^{in} that are unknown. To determine these two parameters, it is sufficient to perform macromechanical tests on uniaxial tension of the monolayer in the direction of the x and y axes.

Basing ourselves on macro- and micromechanical tests, we can determine the elastic modulus of the interphase E^{in} and its volume fraction ν^{in} from Equations (2), (4), and (5) using the following formulas:

$$E^{in} = \frac{E^f \cdot E_y \cdot \left(\left(1 - \nu^f\right) \cdot E^m + \nu^f \cdot E^f - E_x\right)}{\left(\left(\nu^f - 1\right) \cdot E^f - \nu^f \cdot E^m\right) \cdot E_y + E^m \cdot E^f}, \tag{6}$$

$$\nu^{in} = \frac{\nu^f \cdot E^f + \left(1 - \nu^f\right) \cdot E^m - E_x}{E^m - E^{in}}. \tag{7}$$

It follows from experiments of uniaxial tension of the monolayer along the x-axis and the mixture rule that $\mu_{xy} = \mu^f \cdot \nu^f + \mu^m \cdot \nu^m + \mu^{in} \cdot \nu^{in}$, where μ_{xy} is Poisson's ratio for the monolayer in Hooke's law (1); and μ^f, μ^m, and μ^{in} are Poisson's ratios for the fiber, the matrix, and the interphase, respectively. A detailed derivation of an equation similar to this one can be found in the work [48]. From this equality, one can determine the Poisson's ratio of the interphase μ^{in} by the following formula:

$$\mu^{in} = \frac{1}{\nu^{in}}\left(\mu_{xy} - \mu^f \cdot \nu^f - \mu^m \cdot \nu^m\right). \tag{8}$$

If the volume fraction of the interphase has been measured experimentally, its mechanical properties can then be calculated using Equations (6) and (8).

3.2. The Computational Model of the Monolayer with the Interphase

The fibers in the fiberglass monolayer are misoriented relative to the laying axis; therefore, to determine the misorientation of the fibers, the monolayers were separately polymerized and analyzed from images obtained by optical microscopy. Figure 5 shows a longitudinal image of one layer of the polymerized prepreg (monolayer) in transmitted light. The analysis of 100 fibers has shown that the angle of deviation from the laying axis

(misorientation angle) can be up to 3°. In this connection, the computational mesomechanical model of the monolayer is constructed from the possibility of random distribution and misorientation of fibers (see Figure 6). To do this, the location of each fiber and the deviation of the fibers from the laying axis within 3° are randomly set. The fiber diameter is set according to the distribution law shown in Figure 1b. The fraction of fibers is 0.49. This value corresponds to the experimentally determined average value obtained from 50 images of the monolayer cross section (see Figure 1a). The image size for calculating the fiber volume fraction in the monolayer is 100 × 100 μm.

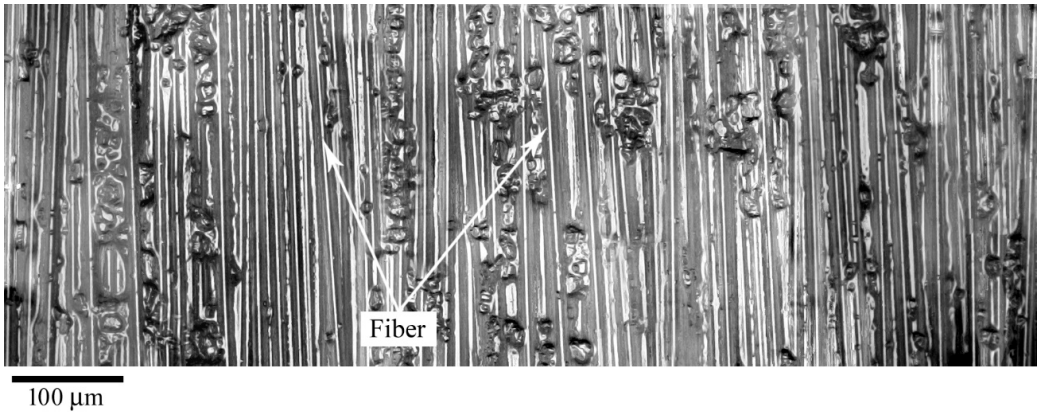

Figure 5. Fiber misorientation in the fiberglass plastic monolayer. The image is obtained by passing light through the monolayer.

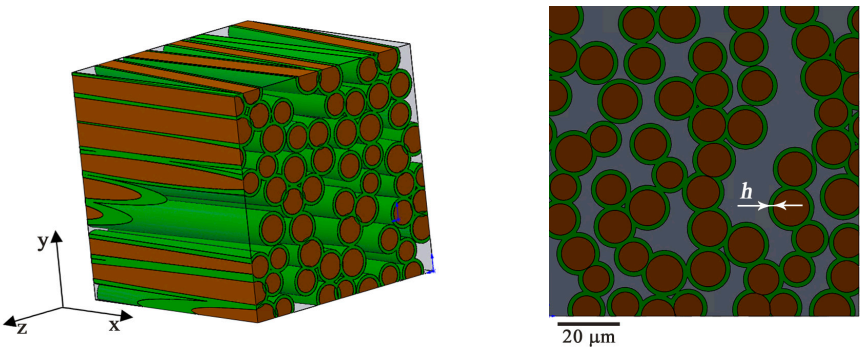

Figure 6. Solid model (**a**,**b**) of the polymer composite monolayer with a 3° fiber misorientation and the interphase thickness h arbitrarily taken equal to 3 μm. The size of the representative volume of the composite is 100 × 100 × 100 μm.

In the construction of the computational model, it is assumed that the interphase connects each fiber with the matrix uniformly along its entire length (see Figure 6). The interphases of adjacent fibers may intersect, thus forming an interphase common to these fibers. It is assumed that there is a perfect adhesive bond at the *interphase–matrix* and *interphase–fiber* contacts. The interphase thickness is set constant for all the fibers regardless of the fiber diameter. The unknown parameters of the interphase are determined by minimizing the deviation of the coefficients E_x, E_y, and μ_{xy} calculated by the computational model from those experimentally determined for the monolayer. These coefficients are calculated for uniaxial tension along and across the fiber laying, i.e., along the x and y axes (see Figure 6), respectively.

3.3. Determination of Monolayer Mechanical Properties

After determining the elastic modulus E^{in}, Poisson's ratio μ^{in}, and the interphase thickness h in the representative volume of the monolayer, it is possible to calculate all

the unknown elastic constants in Hooke's law (1) for the monolayer. Since the compliance matrix in (1) is symmetric, it is necessary to determine 10 elastic constants: E_x, E_y, E_y, E_z, G_{xy}, G_{yz}, G_{xz}, μ_{xy}, μ_{xz}, and μ_{yz}. The values of these quantities are determined from the results of numerical calculations simulating the mechanical loading of the monolayer at the mesoscale.

Deformation is simulated for six cases, such as uniaxial tension along the x, y, and z axes, as well as shear in the xy, xz, and yz planes (see Figure 7). The calculations are made in a quasi-static formulation in ANSYS. The boundary conditions are specified in terms of displacements U_j^k along the k-th face of the monolayer computational model ($k = 1, \ldots, 6$) in the direction of the j coordinate axis ($j = x, y, z$). The limiting value of the load in displacements is set from the condition of ensuring the equivalent macrostrain $\widetilde{\varepsilon}$ to be equal to 0.01. To determine the elastic modulus and Poisson's ratio, tension is simulated along the x, y, and z axes. Faces 2, 3, and 4 coinciding with the coordinate planes (see Figure 7) have zero displacements in the direction of the y, x, and z axes, respectively. To determine the shear moduli, the following boundary conditions are used:

(1) for G_{xy}: $U_y^6 = 1.7$ μm, $U_x^3 = U_y^3 = U_z^3 = U_x^4 = U_z^4 = 0$;
(2) for G_{yz}: $U_z^1 = 1.7$ μm, $U_x^2 = U_y^2 = U_z^2 = U_x^1 = U_y^1 = 0$;
(3) for G_{xz}: $U_z^6 = 1.7$ μm, $U_x^3 = U_y^3 = U_z^3 = U_x^4 = U_y^4 = 0$.

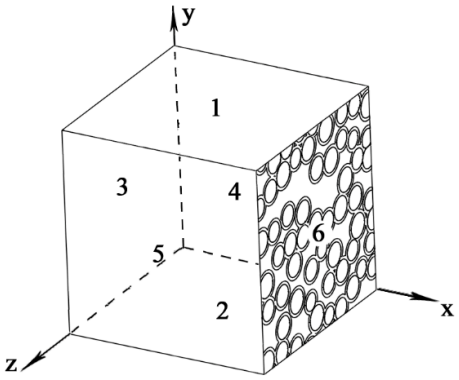

Figure 7. The numbers of the faces of the mesomechanical model for setting the boundary conditions in the simulation of tension and shear. Faces 2, 3, and 4 coincide with the coordinate planes.

3.4. The Computational Model of a Specimen Made from 14-Layer Transversely Reinforced Fiberglass Plastic

The monolayer coefficients in Hooke's law (1) are verified by comparison of experimental and calculated data on the tension of the 14-layer transversely reinforced fiberglass plastic (see Figure 1). In the statement of the tension problem for the cross-reinforced fiberglass plastic at the macroscale, it is considered that there is a perfect adhesive bond between the monolayers of the material. Fourteen layers are identified in the finite element model. They correspond to 14 monolayers of actual fiberglass plastic.

In the statement of the computational problem, zero displacements are set in the direction of the x, y, and z axes to faces 1 to 5 (see Figure 8). For faces 6 to 10, zero displacements are set along the y and z axes, and the limiting displacement is set along the x-axis from the condition of ensuring the equivalent macrostrain $\widetilde{\varepsilon}'$ to be equal to 0.01.

Figure 8 shows the numbers of specimen faces to which boundary conditions are applied. Faces 1 to 10 in this figure correspond to the areas of the specimen clamped in the grips of the device. The monolayer parameters in Hooke's law (1) are indicated for each layer depending on the location of the glass fiber relative to the tension axis. The boundary conditions are specified in terms of displacements $\widetilde{U}_j^l$ along the l-th face of the computational model ($l = 1, \ldots, 10$) in the direction of the j coordinate axis ($j = x, y, z$).

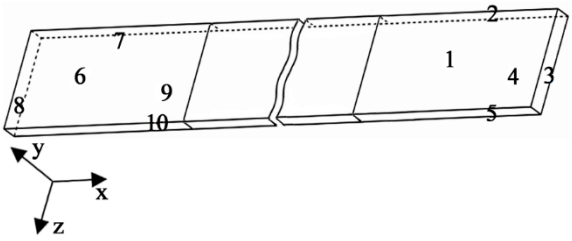

Figure 8. The numbered faces in the model of a 14-layer cross-reinforced fiberglass plastic, used to set boundary conditions for tension simulation.

4. Results and Discussion

4.1. Experimental Data on the Mechanical Properties of the Fiber, the Matrix, and the Interphase Thickness

The elastic modulus and Poisson's ratio of the glass fiber and the matrix are determined from micromechanical tests. The reduced elastic modulus $E*$ of the glass fiber and the matrix is determined from the results of instrumented microindentation. The polymer and the fibers were indented with a Berkovich indenter at loads of 5 and 50 mN, respectively (see Figure 9). Table 1 shows the values of the reduced elastic modulus $E*$ obtained from 20 measurements.

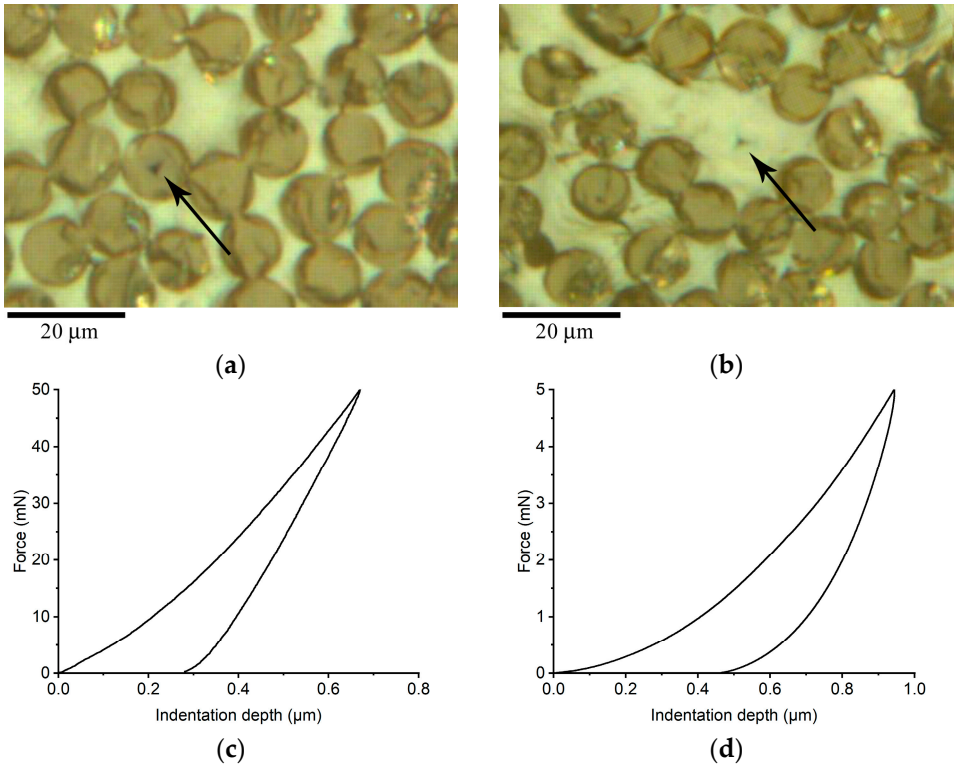

Figure 9. The image of the imprint of a Berkovich indenter on the fiberglass (**a**) at a load of 50 mN and on the polymer matrix (**b**) at a load of 5 mN; typical curves of loading by the Berkovich indenter for the fiberglass (**c**) and the polymer matrix (**d**).

To determine the elastic modulus or Poisson's ratio for the material of the required phase from the microindentation results, the following formula is used [39]:

$$E = \frac{1-(\mu_s)^2}{\frac{1}{E*} - \frac{1-(\mu_i)^2}{E_i}}, \quad (9)$$

where μ_s is the Poisson's ratio of the test specimen; μ_i is the Poisson's ratio of the indenter, equal to 0.07 for diamond [39]; $E*$ is the reduced elastic modulus for the test specimen; and E_i is the elastic modulus for the indenter, equal to $1.14 \cdot 10^6$ N/mm^2 for diamond [39].

Table 1. Mechanical properties of the polymer matrix and the fiberglass.

Material	E^*, GPa	μ_s	E, GPa	Ultimate Strength, MPa	E_x, GPa	E_y, GPa	M_{xy}
Fiberglass	92.6 ± 7.1	0.20 [1]	89.0 ± 6.8 [2]	2135 ± 25	-	-	-
Matrix	4.5 ± 0.3	0.33 [51]	4.0 ± 0.3	-	-	-	-
Unidirectional fiberglass plastic	-	-	-	-	48.7 ± 3.1	14.1 ± 0.4	0.22 ± 0.02

[1] The μ_s value is calculated using the average of the E^* and E values. The formula for determining μ_s is deduced from Equation (9). [2] The elastic modulus of the fiberglass is determined by micromechanical tensile testing.

The elastic modulus E^f of the fiberglass is determined directly from 10 tensile tests for single fiber (see Section 2). The Poisson's ratio μ^f of the fiber is evaluated from (9) and calculated for the experimental values of the reduced elastic modulus of the fiber and its elastic modulus (Table 1).

The experimental thickness of the interphase, h, was measured using dynamic force microscopy (DFM) images based on the frequency of the cantilever oscillation (frequency mode). Figure 10a shows a DFM image of a fiber, matrix, and interphase at an angle of 30° to the composite surface (see Figure 3). Figure 10b shows a linear profile along the minor axis of the ellipse that describes the fiber shape in Figure 10a. After 20 measurements of different fibers, the interphase thickness was found to be 621 ± 53 nm. The average thickness of the interphase was used in the finite element model.

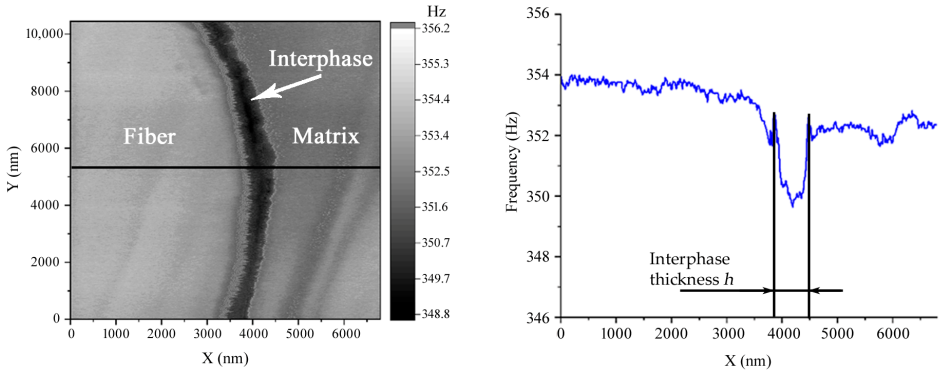

Figure 10. A DFM image of a composite monolayer obtained at a 30° relative to its surface (**a**), and a linear profile (**b**) of the frequency of the cantilever oscillation along the black line in (**a**).

4.2. Determination of the Mechanical Properties of the Interphase

To determine the interphase parameters, a computational model with the fiber volume fraction equal to 0.49 is used (see Section 3.2). Two problems were considered. The first problem had two unknowns: the elastic modulus of the interphase E^{in} and Poisson's ratio μ^{in}. The second problem had three unknowns: the elastic modulus E^{in} of the interphase, Poisson's ratio μ^{in}, and interphase thickness h. These parameters were determined by

varying them using the simplex method, so that the average relative deviation δ_c calculated by Formula (10) becomes less than 5%,

$$\delta_c = \frac{1}{3}\left(\frac{|E_x^s - E_x|}{E^x} + \frac{\left|E_y^s - E_y\right|}{E^y} + \frac{\left|\mu_{xy}^s - \mu_{xy}\right|}{\mu_{xy}}\right) \cdot 100\%, \quad (10)$$

where E_x, E_y, and μ_{xy} are the coefficients in Hooke's law (1) determined from five natural experiments on the tension of unidirectional fiberglass plastic along and across the fiber laying (see Figure 4); E_x^s, E_y^s, and μ_{xy}^s are the coefficients in Hooke's law (1) obtained from the simulation results. The experimental values of E_x, E_y, and μ_{xy} determined in natural experiments are given in Table 1.

To calculate the initial set of values for searching for unknown parameters in the interphase, we used data from Table 1. For the first problem, with known experimental thickness of the interphase, the elastic modulus E^{in} and Poisson's ratio μ^{in} were calculated using Equations (6) and (8). This resulted in an initial set of values of {12.3, 0.02}, where the first number corresponds to E^{in} and the second corresponds to μ^{in}. For the second problem, where the experimental thickness is unknown, we determined the initial set E^{in}, μ^{in}, and ν^{in} using Formulas (6)–(8). As a result, the initial set of values has the following form: {12.3; 0.20; 0.37}, where the first number corresponds to E^{in}, the second corresponds to μ^{in}, and the third corresponds to ν^{in}. The volume fraction of the interphase equal to 0.37 corresponds to the interphase thickness h equal to 1.7 μm, which differs significantly from the experimentally determined value. This indicates that Equations (6) and (7), derived from the mixture model without considering fiber misorientation, are not suitable for determining the average thickness of the interphase. In the initial parameter sets for the first and second problems, the Poisson coefficients for the interphase μ^{in} differed by an order of magnitude, which can be explained by the absence of consideration for fiber misorientation in the calculations.

Table 2 below shows the enumeration of the unknown interphase parameters for two problems using a mesomechanical model. As can be seen from Table 2, the values of the elastic parameters of the interphase are similar when solving the first and second problems. Additionally, the average values of the interphase thickness obtained through simulations and experiments are also similar (with a deviation of 6%). However, the quantity of iterations, consequently determining the duration necessary to ascertain the elastic properties and interphase thickness, is nearly tripled in instances where the thickness is undetermined. So, it took nine iterations to determine the Poisson's ratio μ^{in} and the elastic modulus E^{in} of the interphase when the average thickness of the interphase was experimentally determined. However, it was necessary to use 30 iterations to solve the problem and determine the elastic properties and interphase thickness based only on the elastic properties of structural components and mechanical properties at the macro level. Additionally, solving the second problem required time-consuming changes to the geometric dimensions of the interphase, the creation of contacts, the generation of a new mesh, and other steps, which significantly increased the complexity of solving the second problem.

Table 2. Interphase parameters resulting from the application of the computational model.

The Experimental Value of the Interphase Thickness	E^{in}, GPa	μ^{in}	h, nm	δ_c, %
Known (first problem)	12.7	0.07	621 [1]	4.1
Unknown (second problem)	12.5	0.09	660	4.9

[1] The average thickness of the interphase was determined experimentally using the dynamic force microscopy data.

4.3. Verification of the Mechanical Properties of the Interphase

Since the average thickness of the interface is 621 nanometers, it is not a trivial task to experimentally determine and verify the calculated mechanical properties of the interphase. In this work, we verified the values of the elastic coefficients of the interphase by comparing experimental and calculated data obtained during the tension of the specimen. The scheme of laying the specimen layers was different from the one used to determine the mechanical properties of the interphase. To verify the results, we initially calculated nine elastic constants for the monolayer in Hooke's law, as described in Section 3.3. Table 3 shows the elastic coefficients of the monolayer obtained from simulating five generated computational models. The values of the elastic modulus, Poisson's ratio, and the interphase thickness are provided in Table 2, for the first model in which the size of the interphase was determined experimentally. Further, all results will be presented only for the interphase parameters obtained from solving this first problem. Table 3 also shows the average relative deviation δ of the calculated elastic coefficient of the monolayer from the experimentally determined one.

Table 3. Compliance matrix coefficients in (1) obtained from simulation of five computational models.

		δ, %
E_x, GPa	46.97 ± 0.01	3.6
E_y, GPa	14.88 ± 0.23	5.5
E_z, GPa	15.07 ± 0.30	6.9
G_{xy}, GPa	6.59 ± 0.05	-
G_{yz}, GPa	6.03 ± 0.15	-
G_{xz}, GPa	6.70 ± 0.33	-
μ_{xy}	0.213 ± 0.001	3.2
μ_{xz}	0.213 ± 0.001	3.2
μ_{yz}	0.276 ± 0.015	-

To verify the obtained elastic coefficients of the monolayer, tension of the 14-layer cross-reinforced fiberglass plastic is simulated (see Section 3.4). The elastic coefficients obtained from the simulation are then compared with the results obtained from natural experiments. Table 4 shows the elastic modulus E'_x and Poisson's ratio μ'_{xy} of the 14-layer fiberglass plastic. It can be seen from Table 4 that the average relative deviation of the experimental data from the calculated ones does not exceed 10%. This indicates that the interphase parameters for the first problem (see Table 2) are determined with good engineering accuracy, sufficient to predict the elastic properties of composites made from prepreg monolayers of the fiberglass plastic under study.

Table 4. Experimental and calculated values of the elastic modulus of the 14-layer fiberglass plastic.

	Natural Test	**Simulation**	**δ, %**
E'_x, GPa	29 ± 2	31 ± 1	7
μ'_{xy}	0.10 ± 0.02	0.11 ± 0.01	10

Figure 11 shows an image of the solid model of the fiberglass plastic monolayer containing the interphase, whose parameters were determined from the results of computational experiments at solving the first problem (see Table 2). It is obvious from this figure that, since the interphase is thin, only 621 nm, it is a nontrivial task to perform correct microindentation into it. Figure 12 shows three groups of curves I–III corresponding to different distances to the fiber boundary. Curve group I is located at a distance of 15 μm from the fiber boundary, and it corresponds to the matrix loading curves (see Figure 9d) obtained from microindentation into the fiber-free matrix of the composite. Curve group II

is located at a distance of 5 μm, and it corresponds to the average reduced elastic modulus equal to 11 GPa. Curve group III is located at a distance of 1 to 2 μm, and it corresponds to the average reduced elastic modulus equal to 65 GPa. These data show that the correct determination of the elastic modulus of the interphase by indentation is a nontrivial task due to a too small thickness of the zone [52].

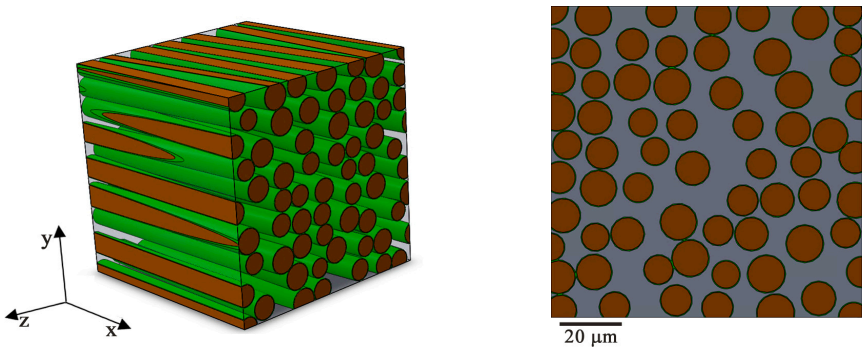

Figure 11. The solid model (**a**,**b**) of the polymer composite monolayer with a fiber misorientation of 3°. The size of the representative volume of the composite is 100 × 100 × 100 μm.

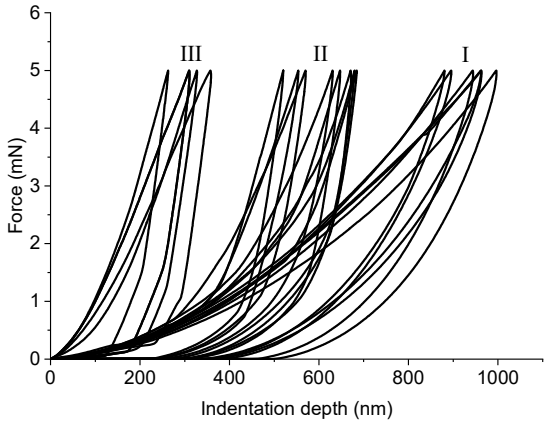

Figure 12. Berkovich indenter loading curves of the polymer matrix in the monolayer of the fiberglass plastic. The group of curves I corresponds to the distance from the indent to the fiberglass boundary equal to 15 μm; II group is 5 μm; III group is between 1 and 2 μm.

Figures 13 and 14 show von Mises stress distribution in the representative volume of the fiberglass plastic monolayer when it is stretched along and across the fiber at the moment of specimen failure. Figure 13b shows that, when tension is along the fibers, the level of the stress state in the interphase significantly exceeds that in the matrix. When tension is across the fibers, the opposite pattern is observed, i.e., the level of the stress state in the matrix significantly exceeds that in the interphase (see Figure 14b). This effect of the direction of tensile force application to the composite along the direction of fiber laying leads to the fact that crack initiation should occur at the boundary between the interphase and the fiber. When the composite is tensioned across the fibers, crack initiation should occur at the interphase–matrix boundary or inside the polymer matrix itself. The results are indirectly confirmed by the fractographic analysis of the images after fracture.

Figure 15 shows the fracture surfaces of the specimens when they are tensioned along and across the fiber laying. Comparing the fracture surfaces shown in Figure 15a,b, one can see qualitatively different fracture patterns. Thus, the fracture surface resulting from composite tension along the fiber laying abounds with fibers free from the matrix. When the composite is tensioned across the fiber laying, free fibers are almost absent.

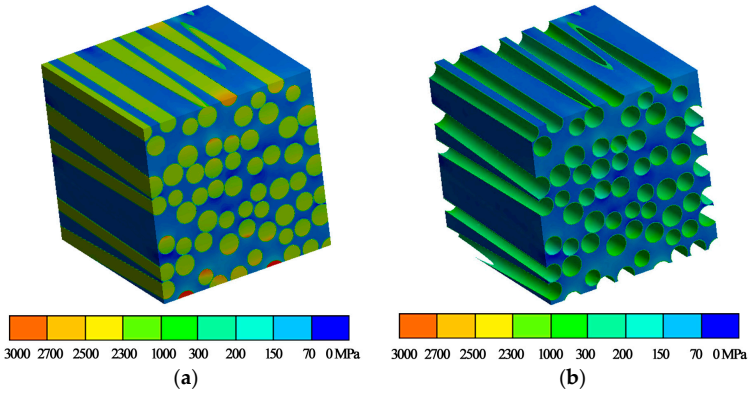

Figure 13. Von Mises stress distribution in the fibers (**a**) and in the interphase (**b**) at the moment of specimen fracture when the specimen is tensioned along the fiber-laying axis.

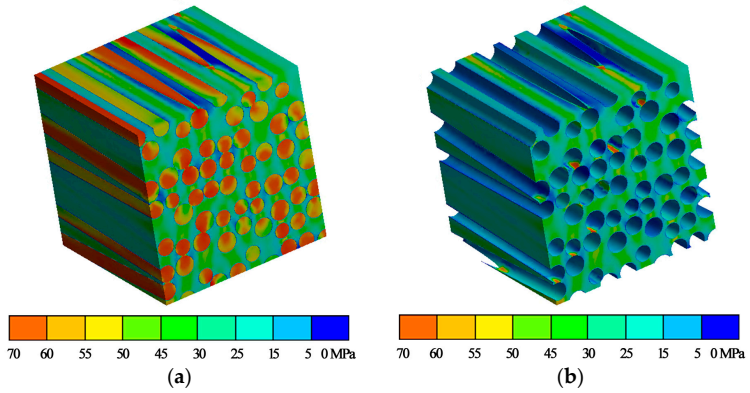

Figure 14. Von Mises stress distribution in the fibers (**a**) and in the interphase (**b**) at the moment of specimen fracture when the specimen is tensioned across the fiber-laying axis.

The results of tensioning the representative volume of the monolayer along the fiber direction (see Figure 13) show that, at the moment of specimen fracture, the average von Mises stress over all the fibers is about 2000 MPa. This agrees well with the experimental results of tensioning a single fiber (see Table 1) and indicates that the composite matrix effectively transfers the load to the glass fibers during fiberglass plastic deformation. The obtained results of simulating the representative volume indicate the need to take into account the interphase when considering the mechanical properties and conditions of polymer composite fracture. In particular, this concerns the simulation of adhesive and cohesive failure at the micro and meso levels. Thus, the absence of the explicit introduction of the interphase into computational models of a polymer composite may cause significant errors in simulating the initiation and evolution of cracks in the composite.

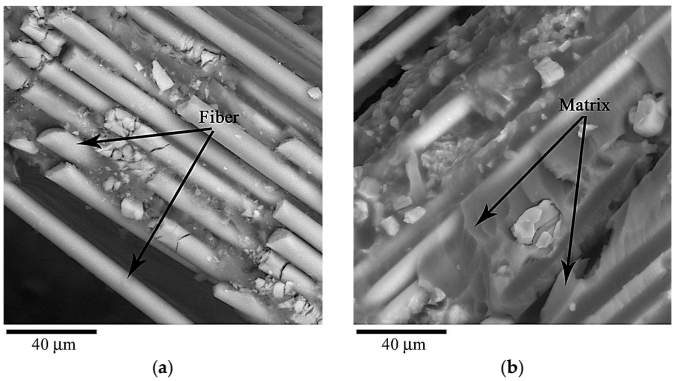

Figure 15. Fracture surface of fiberglass plastic specimens along the fibers and the matrix (**a**) and along the matrix alone (**b**) when specimens are tensioned along (**a**) and across (**b**) the fiber laying.

5. Conclusions

In this study, the mechanical properties and dimensions of the interphase have been determined based on dynamic force microscopy, macro- and micromechanical tests using a computational model of the monolayer of unidirectional fiberglass plastic. In particular, the following results have been obtained:

1. From micromechanical tension and indentation testing of a single fiber, their elastic modulus and Poisson's ratio have been determined. They are 89 GPa and 0.2, respectively.
2. It has been shown that the elastic modulus of the interphase is 12.7 GPa. This significantly exceeds the elastic modulus of the composite matrix, which is 4.0 GPa.
3. The Poisson's ratio of the interphase is 0.07, and this is significantly lower than the Poisson's ratio of the matrix, which is taken equal to 0.33 from reference data.
4. The interphase thickness has been determined using dynamic force microscopy, and it is equal to 621 $\pm$ 53 nm.
5. The use of the mesomechanical model allowed us to calculate the interphase thickness equal to 660 nm. This value corresponds to the acceptable engineering accuracy of determining the parameter, since the deviation is less than 10%. The calculation of the interphase thickness has taken 30 iterations when solving the finite element problem, leading to significant time spent on determining this parameter.
6. On the basis of a computational model of the representative volume of the fiberglass plastic monolayer, its elastic coefficients have been determined. This has made it possible to predict the elastic properties of 14-layer transversely reinforced fiberglass plastic with relative average deviation not exceeding 10%.

Author Contributions: Conceptualization, A.S.; Methodology, A.S.; Validation, A.S., E.S., D.V. and Y.K.; Formal analysis, A.S., E.S., Y.K. and D.V.; Investigation, A.S., E.S., D.V., Y.K., I.S., and V.K.; Writing—original draft preparation, A.S. and E.S.; Writing—review and editing, A.S., E.S. and O.M.; Project administration, E.S. and A.S.; Funding acquisition, E.S. All authors have read and agreed to the published version of the manuscript.

Funding: This research was financially supported by the Russian Science Foundation, project No. 24-29-00703.

Data Availability Statement: Data available upon request.

Acknowledgments: The computing resources at the supercomputer center of the IMM UB RAS, and the equipment of the *Plastometriya* shared research facilities at the IES UB RAS were used in the study.

Conflicts of Interest: The authors declare no conflicts of interest.

References

1. Zhang, B.; Jia, L.; Tian, M.; Ning, N.; Zhang, L.; Wang, W. Surface and Interface Modification of Aramid Fiber and Its Reinforcement for Polymer Composites: A Review. *Eur. Polym. J.* **2021**, *147*, 110352. [CrossRef]
2. Bolt, J.D.; Button, D.P.; Yost, B.A. Ceramic-Fiber-Polymer Composites for Electronic Substrates. *Mater. Sci. Eng. A* **1989**, *109*, 207–211. [CrossRef]
3. Sathishkumar, T.P.; Satheeshkumar, S.; Naveen, J. Glass Fiber-Reinforced Polymer Composites—A Review. *J. Reinf. Plast. Compos.* **2014**, *33*, 1258–1275. [CrossRef]
4. Sethi, S.; Ray, B.C. Environmental Effects on Fibre Reinforced Polymeric Composites: Evolving Reasons and Remarks on Interfacial Strength and Stability. *Adv. Colloid Interface Sci.* **2015**, *217*, 43–67. [CrossRef]
5. Begum, S.; Fawzia, S.; Hashmi, M.S.J. Polymer Matrix Composite with Natural and Synthetic Fibres. *Adv. Mater. Process. Technol.* **2020**, *6*, 547–564. [CrossRef]
6. Saroia, J.; Wang, Y.; Wei, Q.; Lei, M.; Li, X.; Guo, Y.; Zhang, K. A Review on 3D Printed Matrix Polymer Composites: Its Potential and Future Challenges. *Int. J. Adv. Manuf. Technol.* **2020**, *106*, 1695–1721. [CrossRef]
7. Kumar, S.; Graninger, G.; Hawkins, S.C.; Falzon, B.G. A Nanostructured Cellulose-Based Interphase Layer to Enhance the Mechanical Performance of Glass Fibre-Reinforced Polymer Composites. *Compos. Part A Appl. Sci. Manuf.* **2021**, *148*, 106475. [CrossRef]

8. Li, Y.; Wang, Q.; Wang, S. A Review on Enhancement of Mechanical and Tribological Properties of Polymer Composites Reinforced by Carbon Nanotubes and Graphene Sheet: Molecular Dynamics Simulations. *Compos. Part B Eng.* **2019**, *160*, 348–361. [CrossRef]
9. Chen, J.; Wan, L.; Ismail, Y.; Hou, P.; Ye, J.; Yang, D. Micromechanical Analysis of UD CFRP Composite Lamina under Multiaxial Loading with Different Loading Paths. *Compos. Struct.* **2021**, *269*, 114024. [CrossRef]
10. Gu, Y.; Li, M.; Wang, J.; Zhang, Z. Characterization of the Interphase in Carbon Fiber/Polymer Composites Using a Nanoscale Dynamic Mechanical Imaging Technique. *Carbon* **2010**, *48*, 3229–3235. [CrossRef]
11. Bashir, M.A. Use of Dynamic Mechanical Analysis (DMA) for Characterizing Interfacial Interactions in Filled Polymers. *Solids* **2021**, *2*, 108–120. [CrossRef]
12. Gan, Y.X. Effect of Interface Structure on Mechanical Properties of Advanced Composite Materials. *Int. J. Mol. Sci.* **2009**, *10*, 5115–5134. [CrossRef]
13. Kashfipour, M.A.; Mehra, N.; Zhu, J. A Review on the Role of Interface in Mechanical, Thermal, and Electrical Properties of Polymer Composites. *Adv. Compos. Hybrid Mater.* **2018**, *1*, 415–439. [CrossRef]
14. Pukánszky, B. Influence of Interface Interaction on the Ultimate Tensile Properties of Polymer Composites. *Composites* **1990**, *21*, 255–262. [CrossRef]
15. Kotiveerachari, B.; Reddy, A.C. Interfacial Effect on the Fracture Mechanism in GFRP Composites. In Proceedings of the CEMILAC Conference, Ministry of Defence, Bangalore, India, 20–21 August 1999; pp. 85–87.
16. Wang, X.; Zhao, X.; Wu, Z. Fatigue Degradation and Life Prediction of Basalt Fiber-Reinforced Polymer Composites after Saltwater Corrosion. *Mater. Des.* **2019**, *163*, 107529. [CrossRef]
17. Muyzemnek, A.Y.; Ivanova, T.N.; Kartashova, E.D. A Comparison of Experimental and Computation Results of Finding Effective Characteristics of Elastic Properties of Polymer Layered Composites from Carbon and Glass Fabrics. *PNRPU Mech. Bull.* **2021**, *2*, 88–105. [CrossRef]
18. Smirnov, A.; Smirnova, E.; Khudorozhkova, Y. Constructing a Two-Level Computational Model of Cross-Ply Fiberglass-Reinforced Plastic from Micromechanical Testing. *Polym. Polym. Compos.* **2022**, *30*, 09673911221112414. [CrossRef]
19. Rodenas, T.; Luz, I.; Prieto, G.; Seoane, B.; Miro, H.; Corma, A.; Kapteijn, F.; Llabrés I Xamena, F.X.; Gascon, J. Metal-Organic Framework Nanosheets in Polymer Composite Materials for Gas Separation. *Nat. Mater.* **2015**, *14*, 48–55. [CrossRef]
20. Nan, N.; Wang, J.; Eckstein, A.A. FIB-SEM Three-Dimensional Tomography for Characterization of Carbon-Based Materials. *Adv. Mater. Sci. Eng.* **2019**, *2019*, 8680715. [CrossRef]
21. Koch, T.; Salaberger, D.; Zankel, A.; Reingruber, H.; Steiger-Thirsfeld, A.; Voronko, Y.; Seidler, S. Methods for Characterizing the 3-D Morphology of Polymer Composites. *Macromol. Symp.* **2012**, *315*, 115–124. [CrossRef]
22. Maire, E.; Withers, P.J. Quantitative X-Ray Tomography. *Int. Mater. Rev.* **2014**, *59*, 1–43. [CrossRef]
23. Niu, Y.-F.; Yang, Y.; Wang, X.-R. Investigation of the Interphase Structures and Properties of Carbon Fiber Reinforced Polymer Composites Exposed to Hydrothermal Treatments Using Peak Force Quantitative Nanomechanics Technique. *Polym. Compos.* **2018**, *39*, E791–E796. [CrossRef]
24. Wu, Q.; Li, M.; Gu, Y.; Wang, S.; Wang, X.; Zhang, Z. Reaction of Carbon Fiber Sizing and Its Influence on the Interphase Region of Composites. *J. Appl. Polym. Sci.* **2015**, *132*, 41917. [CrossRef]
25. Garcea, S.C.; Wang, Y.; Withers, P.J. X-Ray Computed Tomography of Polymer Composites. *Compos. Sci. Technol.* **2018**, *156*, 305–319. [CrossRef]
26. Jiang, N.; Yu, T.; Li, Y.; Pirzada, T.J.; Marrow, T.J. Hygrothermal Aging and Structural Damage of a Jute/Poly (Lactic Acid) (PLA) Composite Observed by X-Ray Tomography. *Compos. Sci. Technol.* **2019**, *173*, 15–23. [CrossRef]
27. Sinchuk, Y.; Kibleur, P.; Aelterman, J.; Boone, M.N.; Van Paepegem, W. Variational and Deep Learning Segmentation of Very-Low-Contrast X-ray Computed Tomography Images of Carbon/Epoxy Woven Composites. *Materials* **2020**, *13*, 936. [CrossRef]
28. Xue, H.; He, J.; Zhang, J.; Xue, Y. Approach for Obtaining Material Mechanical Properties in Local Region of Structure Based on Accurate Analysis of Micro-Indentation Test. *Chin. J. Mech. Eng. (Engl. Ed.)* **2021**, *34*, 130. [CrossRef]
29. Broitman, E. Indentation Hardness Measurements at Macro-, Micro-, and Nanoscale: A Critical Overview. *Tribol. Lett.* **2017**, *65*, 23. [CrossRef]
30. Fischer-Cripps, A.C. Critical Review of Analysis and Interpretation of Nanoindentation Test Data. *Surf. Coatings Technol.* **2006**, *200*, 4153–4165. [CrossRef]
31. Smirnov, A.; Smirnova, E.; Konovalov, A.; Kanakin, V. Using the Instrumented Indentation Technique to Determine Damage in Sintered Metal Matrix Composites after High-Temperature Deformation. *Appl. Sci.* **2021**, *11*, 10590. [CrossRef]
32. Smirnov, S.V.; Smirnova, E.O. A Technique for Determining Coefficients of the "Stress-Strain" Diagram by Nanoscratch Test Results. *J. Mater. Res.* **2014**, *29*, 1730–1736. [CrossRef]
33. Eskandari, S.; Carman, G.P.; Case, S. Evaluating the Influence of Fiber Coatings on the Compression Strength of a Unidirectional Polymer Composite. *J. Compos. Mater.* **1996**, *30*, 1958–1976. [CrossRef]
34. Pawlik, M.; Le, H.; Lu, Y. Effects of the Graphene Nanoplatelets Reinforced Interphase on Mechanical Properties of Carbon Fibre Reinforced Polymer—A Multiscale Modelling Study. *Compos. Part B Eng.* **2019**, *177*, 107097. [CrossRef]

35. Wang, M.; Hang, X. Finite Element Analysis of Residual Stress Distribution Patterns of Prestressed Composites Considering Interphases. *Materials* **2023**, *16*, 1345. [CrossRef]
36. Riaño, L.; Chailan, J.F.; Joliff, Y. Evolution of Effective Mechanical and Interphase Properties during Natural Ageing of Glass-Fibre/Epoxy Composites Using Micromechanical Approach. *Compos. Struct.* **2021**, *258*, 113399. [CrossRef]
37. Fankhänel, J.; Arash, B.; Rolfes, R. Elastic Interphase Properties of Nanoparticle/Epoxy Nanocomposites: A Molecular Dynamics Study. *Compos. Part B Eng.* **2019**, *176*, 107211. [CrossRef]
38. Shin, H.; Chang, S.; Yang, S.; Youn, B.D.; Cho, M. Statistical Multiscale Homogenization Approach for Analyzing Polymer Nanocomposites That Include Model Inherent Uncertainties of Molecular Dynamics Simulations. *Compos. Part B Eng.* **2016**, *87*, 120–131. [CrossRef]
39. *ISO 14577-1-2002*; Metallic Materials—Instrumented Parameters—Part 1: Test Method. ISO: Geneva, Switzerland, 2002.
40. Haritos, G.K.; Hager, J.W.; Amos, A.K.; Salkind, M.J.; Wang, A.S.D. Mesomechanics: The Microstructure-Mechanics Connection. *Int. J. Solids Struct.* **1988**, *24*, 1081–1096. [CrossRef]
41. Bobzin, K.; Bagcivan, N.; Parkot, D.; Kashko, T. Calculation of Effective Properties of Textile Reinforced Aluminum Alloy by a Two-Step Homogenization Procedure. *Comput. Mater. Sci.* **2010**, *47*, 801–806. [CrossRef]
42. Krishnan, P. *Evaluation and Methods of Interfacial Properties in Fiber-Reinforced Composites*; Elsevier Ltd.: Amsterdam, The Netherlands, 2018; ISBN 9780081022924.
43. Smirnov, S.V.; Konovalov, A.V.; Myasnikova, M.V.; Khalevitsky, Y.V.; Smirnov, A.S.; Igumnov, A.S. A Hierarchial Modeling of Stress-Strain State of Multiphase Material Subjected to Uniaxial Loading. *AIP Conf. Proc.* **2016**, *1785*, 040066. [CrossRef]
44. Younes, R.; Hallal, A.; Fardoun, F.; Hajj, F. Comparative Review Study on Elastic Properties Modeling for Unidirectional Composite Materials. *Compos. Their Prop.* **2012**, *17*, 391–408. [CrossRef]
45. Gilabert, F.A. An Efficient Anisotropization Technique to Transform Isotropic Nonlinear Materials into Unidirectional and Bidirectional Composites. *Mater. Des.* **2021**, *206*, 109772. [CrossRef]
46. Kilikevičius, S.; Kvietkaitė, S.; Žukienė, K.; Omastová, M.; Aniskevich, A.; Zeleniakienė, D. Numerical Investigation of the Mechanical Properties of a Novel Hybrid Polymer Composite Reinforced with Graphene and MXene Nanosheets. *Comput. Mater. Sci.* **2020**, *174*, 109497. [CrossRef]
47. Arora, G.; Pathak, H. Modeling of Transversely Isotropic Properties of CNT-Polymer Composites Using Meso-Scale FEM Approach. *Compos. Part B Eng.* **2019**, *166*, 588–597. [CrossRef]
48. Egorikhina, E.; Bogovalov, S.V.; Tronin, I.V. Determination of Mechanical Characteristics of Unidirectional Fiber Composites. *Phys. Procedia* **2015**, *72*, 66–72. [CrossRef]
49. Resnyansky, A.D.; Science, D.; Romenski, E. Using a Homogenization Procedure for Prediction of Material Using a Homogenization Procedure for Prediction of Material Properties and the Impact Response of Unidirectional. In Proceedings of the the 11th International Conference on Composite Materials, Gold Coast, Australia, 14–18 July 1997; Volume II, pp. 4–6.
50. Sharma, B.B.; Sharma, R. Young's Modulus of Reinforced Composites. *Adv. Compos. Mater.* **1992**, *2*, 277–288. [CrossRef]
51. Singh, P.K.; Modanwal, R.P.; Kumar, D. Fabrication and Mechanical Characterization of Glass Fiber/Al_2O_3 Hybrid-Epoxy Composite. *Sadhana-Acad. Proc. Eng. Sci.* **2021**, *46*, 32. [CrossRef]
52. Hardiman, M.; Vaughan, T.J.; McCarthy, C.T. A Review of Key Developments and Pertinent Issues in Nanoindentation Testing of Fibre Reinforced Plastic Microstructures. *Compos. Struct.* **2017**, *180*, 782–798. [CrossRef]